REMOTE SENSING OF THE CHINA SEAS AT ORSI/OUC

Ming-Xia HE, Kan Zeng, Haihua Chen, Tinglu Zhang, Lianbo Hu,
Zhishen Liu, Songhua Wu, Chaofang Zhao, Lei Guan, Chuanmin Hu

Ocean Remote Sensing Institute (ORSI), Ocean University of China (OUC)
National Laboratory for Ocean Remote Sensing, Ministry of Education of China
Email: mxhe@orsi.ouc.edu.cn; hucm@orsi.ouc.edu.cn

ABSTRACT We present an overview on the observation and research for the China seas using both field experiments and multi-sensor satellite data at ORSI/OUC, covering two topics: (1) Spatial and temporal distribution of internal waves in the China Seas and retrieval of internal wave parameters; (2) Retrieval, validation, and cross-comparison of multi-sensor ocean color data as well as ocean optics *in situ* experiments in the East China Sea. We also present an incoherent Doppler wind lidar, developed by ORSI, and its observation for marine-atmospheric boundary layer.

KEY WORDS: Remote sensing, Internal wave, Ocean color, Wind lidar, China Seas

1. INTRODUCATION

Remote sensing at ORSI/OUC covers two major topics from satellite to laser technology, of which the former includes: Interactions between the sea surface and the electromagnetic waves (visible, infrared and microwave); Ocean-atmosphere radiance transfer theory; Algorithms for retrieving ocean parameters from satellite data; Image processing and pattern recognition; Development of new concept of the next-generation satellite sensors; Applications of multi-sensor satellite data to the interdisciplinary studies of the ocean; Development of marine GIS. The laser remote sensing includes: Underwater laser transmission; Laser induced seawater fluorescence; Compact lidar technique and measurement of shallow water topography, sea surface wind field and other environmental parameters of the ocean.

Here we report the most recent results from these research topics.

2. INTERNAL WAVE

We studied the spatial-temporal distribution of internal waves, the retrieval of internal wave parameters, in particular the amplitude of internal waves from SAR imagery, the validation of internal waves from Envisat/ASAR through field measurements in the East China Sea, the distribution of internal wave amplitudes in the China Seas using retrieval methods and software developed at ORSI (ORSIW), and the automatic extraction of internal wave signatures from SAR imagery as well as the simulation of SAR image with internal wave signature and the numerical simulation of internal waves in the northern South China Sea.

2.1 Spatial-temporal distribution of internal waves in the China Seas

Historically, *in situ* data of internal waves in the China seas are sparse, while many internal waves (IW) are observed in the South China Sea, East China Sea and Yellow Sea from ERS-1 and ERS-2 imagery (Hsu et al., 2000; Jackson and Apel, 2004).

From approximately 15 thousand satellite images (>50% from SAR and optical imagery) acquired between 1994 and 2004, about 800 images were found to contain internal wave signatures, where the spatial distribution is presented in Fig. 1. This large number of images ensures the rationality of the statistics. According to the generation mechanism of internal waves, the China seas are roughly divided into 5 areas in the Yellow Sea (YS), East Sea (ES), Taiwan waters (TW), DongSha Island waters (DI) and Hainan Island waters (HI), respecitvely. Fig.2 shows the multi-year monthly distribution of internal waves in the 5 areas. No internal wave was observed in the areas of YS, ES, and HI in winter. In all areas, most internal waves occur in summer. These results are generally consistent to the bathymetry, pycnocline properties and spring tide timing in the China seas (Editorial Board For Marine Atlas, 1992).

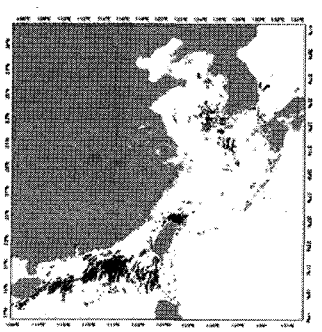

Fig. 1. Multi-year distribution of internal waves.

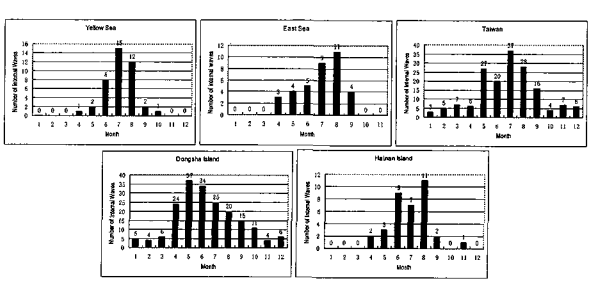

Fig.2. Monthly distribution of internal wave occurrence.

2.2 Internal wave amplitude from SAR imagery

Only a handful of papers on amplitude retrieval have been published in last 25 years (Apel, 2003; Small et al.,1999; Zheng et al., 2001) on two methods, yet no application software is available.

By introducing a modification factor and adopting a parameterized continuously stratified buoyancy frequency, a new method based on the solitary wave solution of KdV equation has been proposed here:

$$a_0 = n\frac{24H^3}{\lambda^2\gamma}$$

where a_0 is the IW amplitude, λ is the IW characteristic width, H is the water depth, γ is a nonlinear parameter, and n is a modification factor related with H and λ.

In theory, the conditions in the shallow waters of the China Seas may not meet the requirement of KdV equation. By inducing the modification factor, n, which is related to the local bathymetry and the IW width, we have greatly improved original relation between a_0 and λ, as validated through field experiments

To extract λ, two methods were used: (1) Direct regression by $\Delta\sigma_0 = A_2 \sec h^2(2\theta/\lambda)\tanh(2\theta/\lambda)$ (Zheng, 2001); (2) Regression and use of Empirical Mode Decomposition (EMD) (Huang, 1998) as a filter to extract low modulation signatures of IW (Zeng, 2004).

Fig. 3 shows the IW amplitude retrieved from an ERS-2 SAR image acquired in the South China Sea northeast off Dongsha atoll on 26 April 2000 during ASIAEX (Asia International Acoustic Experiment).

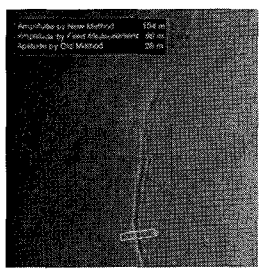

Fig. 3. IW and its amplitude from an ERS-2 SAR image.

The results have been validated through ASIAEX and other experiments in the South China Sea (Yang, 2004; and 10 other published papers). User friendly software has also been developed, from which the distribution IW amplitude was obtained (Fig. 4).

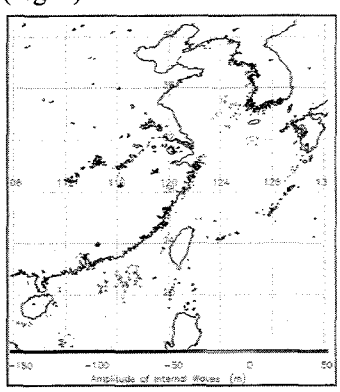

Fig.4 Distribution of IW amplitude in the China Seas.

2.3 First IW validation experiment in the China Sea

A field experiment was conducted in the area east off Zhoushan Island from 25 April to 7 May 2003, when Envisat/ASAR observations were available. The *in situ* instruments included TR7 thermistor string and 7 Starmon mini thermistors, CTD, ADCP, S4 wave recorder, wind meter, three-cup anemometer, electro-magnetic current meter, and a Secchi Disc. The comparison results are presented in table 1 and Fig. 5. The amplitude of leading internal soliton is 5.5 m from the measurements by thermistor string. The left image in fig. 5 is an internal wave packet observed by the thermistor string on 4 May 2003. The right image is the same internal wave packet observed by the Envisat ASAR 6.5 hours late.

γ	λ m	Measured a_0 m	old method a_0 m	Relative Error	new Method a_0 m	Relative Error
6	360	5.5	0.67	88%	4.4	20%

Table 1. Validation of the amplitudes of internal wave retrieved from SAR image with the data acquired during the Zhoushan field experiment.

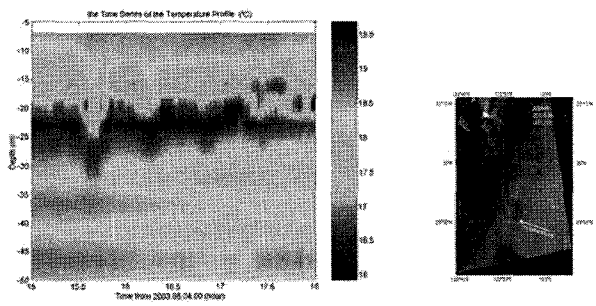

Fig. 5. (left) The IW packet observed by the thermistor string; (right) The same IW packet observed by the Envisat ASAR 6.5 hours later.

2.4 Automatic extraction of IW features from SAR imagery

The algorithm is based on the stationary wavelet transform, which is applicable for large areas (e.g., 8000 x 8000) and has better performance than discrete wavelet transform (DWT) (Rodenas, 1998). Fig. 6 shows an example by applying this new method to an ERS-2 (21.35N, 117.767E) SAR image.

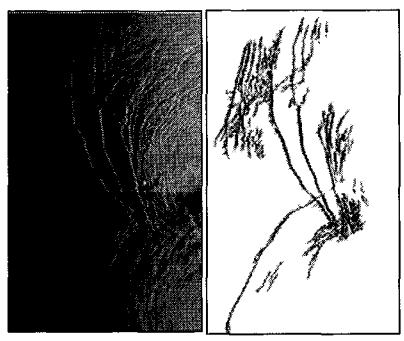

Fig.6. An SAR image (left) and the extracted IW features (right).

3. Ocean color

The East China Sea is a typical case-2 water (turbid water) because of the discharges from the Yangtze River and the Yellow River and other terrestrial runoff. Existing operational atmospheric and bio-optical algorithms yielded large errors in the west of 125E (up to 1000% in chlorophyll retrieval, He et al., 2000).

3.1 Ocean optics *in situ* experiment

Two filed experiments were carried out, respectively, from 17 to 29 April 2006 in the Yellow Sea and from 27 April 27 to 28 May 2005 in the East China sea. Downwelling irradiance (Ed)above surface and upwelling radiance (Lu) near surface were measured by HTSRB. Lu(z) and Ed(z) were also measured by SAM8185 and SAM5018, respectively. Absorption and attenuation coefficients were profiled by an AC-S instrument. Phytoplankton pigments and CDOM absorption spectra were obtained using a U/V spectrophotometer (Carry100, Varian Inc.). Aerosol properties were measured with a skyradiometer (PREDE Co., Ltd, Japan) and an Aerosol Lidar built in house.

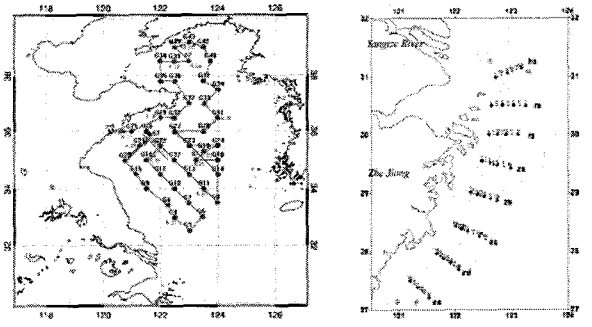

Fig.7. Stations and transects of the two experiments in the Yellow Sea (left) and the East Sea (right).

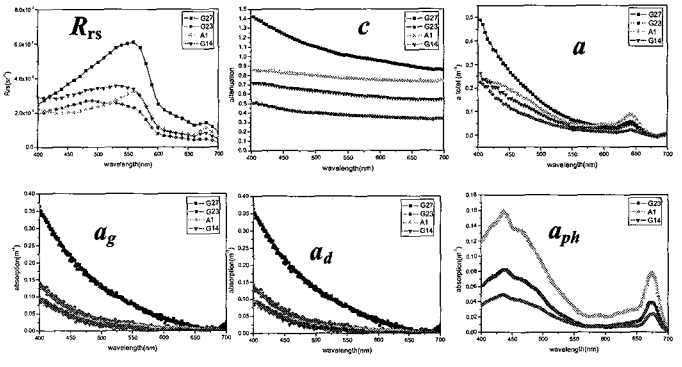

Fig.8. Optical properties from stations G27-G23-A1-G14.

3.2 Optical characteristics in the Yellow Sea

Fig.8 shows examples of theoptical properties along the G27-G23-A1-G14 transect (Fig.7), including remote sensing reflectance (R_{rs}) attenuation and absorption coefficients, absorption coefficients of CDOM, detritus and phytoplankton pigment. The sum of a_g, a_d and a_{ph} is consistent with the total absorption obtained from the AC-S. Fig. 9 further shows the attenuation and absorption profiles at 675nm at A1 and G14 stations.

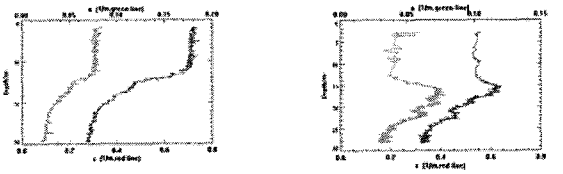

Fig. 9. Profiles of attenuation and absorption coefficients

3.3 Validation of MERIS data in the Yellow Sea

R_{rs} was derived from ENVISAT MERIS Level-1 data using BEAM (MERIS Case-2 Water FUB/WeW Processor), and compared with those determined from *in situ* during 17-29 April 2006. Fig. 10 shows the MERIS RGB image, chlorophyll concentration image, and comparison of R_{rs} and total absorption at several stations. The MERIS total absorption was derived from R_{rs} with a QAA algorithm.

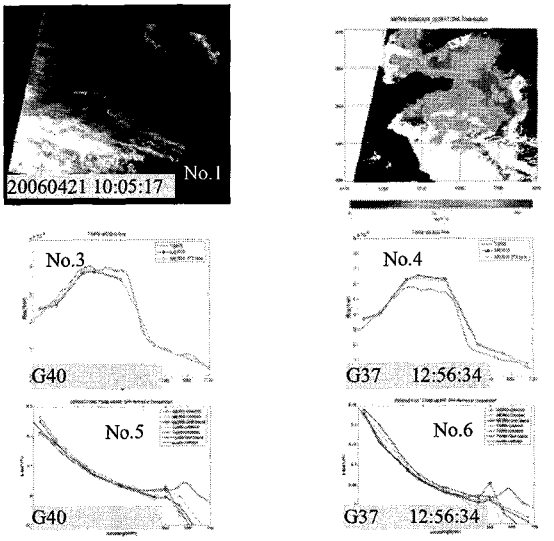

Fig.10. Validation of MERIS data.

Site	FUB/WeW (mg/m^3)	In-situ (mg/m^3)	Relative error %
G40	0.7936	0.6756	17.47%
G37	0.9188	0.8724	5.32%
G34	0.4663	0.1974	136.22%

Table 2: Comparison of chlorophyll concentration.

4. WIND LIDAR

Although there are several ways of measuring wind from satellites, only the active Doppler wind LIDAR has the potential to provide the 3-D data globally. In addition, a Doppler wind LIDAR will not only provide wind data, but also has the potential to provide ancillary information on cloud top heights, vertical distribution of cloud, and aerosol properties as by-products. In the past years ORSI has developed a mobile Doppler wind LIDAR based on

the direct detecting technique using iodine filters (Liu et al., 1997).

4.1 The instrument

The schematic diagram and compact system are shown in Fig. 11. A seed injected Nd:YAG pulse laser generates a pulsed output with narrow linewidth and stable frequency at 532 nm. Two iodine filters are used to lock the transmitter laser frequency and to discriminate the Doppler frequency shift. The system operates with a scanner providing full sky coverage, and a narrow-band interference filter for rejecting daylight.

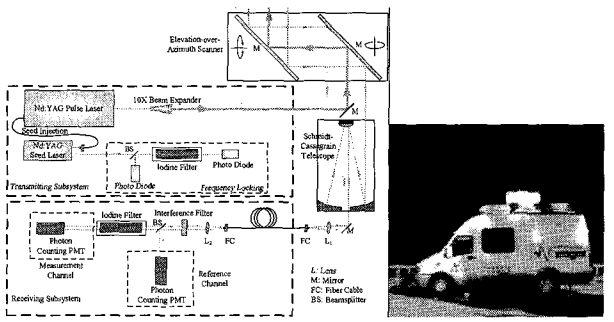

Fig.11 Schematic diagram of the LIDAR and the compact mobile system.

4.2 Wind Measurements

The Doppler LIDAR operates at an elevation of 65° and four azimuths of east, south, west, north, and zenith, respectively. Integration time is 300 s. LIDAR wind data were compared with those from an sonde at a meteorological station. The horizontal distance between the two instruments is 900 m.

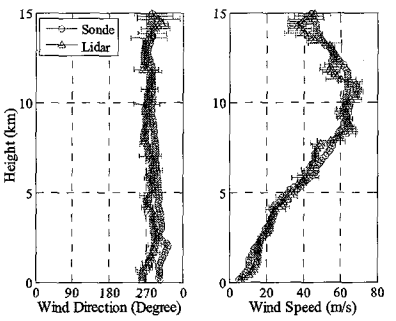

Fig.12. LIDAR versus sonde measurements on 21 April 2005 (sunny day), from 20:20 to 20:50 and 19:15 to 19:55, respectively.

Fig. 12 shows the comparison results. As expected, the agreement of the wind direction above 2 km is better than that below 2 km, due to 900-m distance between the sonde and the lidar measurements.

4.3 Marine Atmospheric Boundary Layer

Aerosol backscattering/scattering ratio was also measured by this LIDAR. The height of the marine atmospheric boundary layer (MABL) and cloud could be derived from the aerosol backscattering/scattering ratio profiles. Fig. 13 shows an example of the measurements. The combination of LIDAR and SAR measurements for the retrieval of wind, MABL parameters, and shallow water topography is ongoing at ORSI.

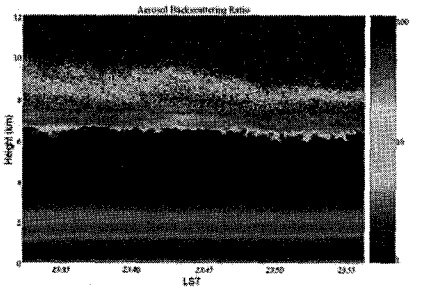

Fig. 13. Backscattering/ scattering ratio obtained on 7 May 2006 from Qingdao.

5. CONCLUSION AND ACKNOWLEDGEMENTS

Remote sensing at ORSI/OUC covers a variety of topics from passive to active techniques. The future plans are to compile an atlas of internal waves in the China Seas, to improve ocean color retrievals in the China Seas, to commercialize the wind LIDAR system.

The research was supported by the National Natural Science Foundation of China (NSFC), '985 Program' of the Ministry of Education of China, Hi-tech Research and Development Program of China, China Meteorological Agency, and ESA-MOST Dragon program.

6. REFERENCES

Apel, J.P., 2003. A new analytical model for internal solitions in the ocean", *J. Phys. Oceanogr.*.33, pp.2247-2269

Editorial Board For Marine Atlas, 1992. "Marine atlas of Bohai Sea, Yellow Sea, East China Sea (Hydrology)", *China Ocean Press*, Beijing, China, pp.524

Hsu, M.K., A.K. Liu and C. Liu, 2000. A study of internal waves in the China Seas and Yellow Sea using SAR. *Continental Shelf Research*, 20, pp.389-410

Jackson, C.R., and J. Apel, 2004. An atlas of internal solitary-like waves and their properties, second edition, *http://www.internalwaveatlas.com/Atlas_index.html*.

He, M-X., et al. Retrial Chlorophyll from Remote-Sensing reflectance in the China seas. *Applied Optics*. 39(15), pp.2467-2474,2000

Huang, N.E., et al., 1998. The empirical mode decomposition and Hilbert spectrum for nonlinear and nonstationary time series analysis. *Porc. Roy. Soc. London A*, vol. 454, pp. 903-995

Rodenas, J.A., and Garello, R., 1998. Internal wave detection and location in SAR images using wavelet transform. *IEEE Trans. on Geosci.and RS.* 36:494-1507.

Small, J., et al, 1999. Observations of Large Amplitude Internal Waves at the Malin Shelf Edge during SESAME 1995. *Cont. Shelf Res.*.19, pp.1389-1436.

Zeng, K., M-X He, 2004. A simple boundary process technique for empirical mode decomposition. *IGARSS '04.* 6:4258-4261.

Zheng, Q., et al, 2001. Theoretical Expression for an Ocean Internal Soliton Synthetic Aperture Radar Image and Determination of the Soliton Characteristic Half Width. *J. Geophys. Res.*. 106:31,415-31,423.

Zhi-Shen Liu, et al., 1997, An incoherent Doppler lidar for ground-based atmospheric wind profiling. *Appl. Phys.* B 64, 561-566.